DOI: 10.1002/ejic.201001053

The Hydrogenase Subcomplex of the NAD$^+$-Reducing [NiFe] Hydrogenase from *Ralstonia eutropha* – Insights into Catalysis and Redox Interconversions

Lars Lauterbach,[a][‡] Juan Liu,[b][‡] Marius Horch,[c][‡] Phillip Hummel,[c] Alexander Schwarze,[a] Michael Haumann,[d] Kylie A. Vincent,[b] Oliver Lenz,[a] and Ingo Zebger*[c]

Keywords: Hydrogen / Enzyme catalysis / [NiFe] hydrogenase / IR spectroscopy / Redox chemistry / Electrochemistry / Metabolism

The O_2-tolerant, NAD$^+$-reducing soluble [NiFe] hydrogenase (SH) from *Ralstonia eutropha* H16, HoxHYFUI_2, is a complex enzyme, harboring multiple redox cofactors: a [NiFe] active site, an electron relay of iron-sulfur clusters, and two noncovalently bound flavin mononucleotides (FMN). The interplay and functional role of these cofactors is so far not understood in detail. In the present study, the isolated HoxHY module was investigated, which represents the smallest active subcomplex of a [NiFe] hydrogenase. Direct electrochemical studies and solution assays showed that the as-isolated HoxHY is initially catalytically inactive, but after reductive activation at low potentials, exhibits both H_2 oxidation and H^+ reduction, consistent with the role of the SH in bidirectional catalysis. The overpotential relative to $E(2H^+/H_2)$ is minimal, facilitating coupling of the closely spaced $2H^+/H_2$ and NAD$^+$/NADH half reactions in the SH. Methyl viologen reduction assays revealed that H_2 oxidation by HoxHY is enhanced on addition of excess FMN, in line with results from optical spectroscopy which indicate that FMN is present at substoichiometric levels in as-isolated HoxHY. X-ray absorption spectroscopy suggested one 4Fe4S cluster in addition to the active site in HoxHY. FTIR investigations confirmed that the active site iron atom has a "standard" ligation, i.e., one CO and two cyanide ligands. At least two novel oxidized states were detected by FTIR, both of which could be reductively activated by artificial electron donors, such as dithionite, and by the native electron donor H_2 in the presence of additional FMN. The flavin cofactor also appears to stabilize the active site, providing further evidence for its importance in HoxHY. All reduced states of the [NiFe] site previously identified for standard [NiFe] hydrogenases and for the native SH within living cells were detected in FTIR spectra of HoxHY with the exception of the intermediate Ni_a-C species. Electrochemical experiments show that incubation of active HoxHY with O_2 at high potentials causes slow inactivation, but activity is recovered within seconds at potentials below –170 mV at 30 °C, even in the presence of 2 % O_2. This behavior is consistent with the HoxHY moiety of the SH remaining active in the presence of O_2 at the potential of the NAD$^+$/NADH pool in vivo.

Introduction

Hydrogenases catalyze the reversible heterolytic cleavage of dihydrogen.[1] According to the metal content of their active sites they are classified as [FeFe], [NiFe], and [Fe] hydrogenases,[2] all of which harbor nonproteinaceous diatomic ligands on Fe. In the case of [NiFe] hydrogenases, the active site nickel is coordinated to the protein matrix by thiolate groups of four cysteine residues, two of which serve as bridging ligands to the iron. Additional coordination of the iron by one carbonyl and two cyanide ligands maintains this atom in a low-spin Fe^{II} state. Most hydrogenases are inhibited by O_2. For [FeFe] hydrogenases, exposure to O_2 usually leads to irreversible damage of the active site,[3,4] whereas for most [NiFe] hydrogenases, reaction with O_2 is largely reversible and leads to a mixture of two inactive states. Anaerobic oxidation at high potentials or incubation with O_2 under conditions where sufficient electrons are available, generates the so called "ready" Ni_r-B form. In this state the enzyme has a hydroxide ligand in the bridging position between nickel and iron which can be rapidly removed by reductive activation.[5–8] Reduction with H_2 converts the Ni_r-B state into the active Ni_a-C state with a bridging hydride ligand.[9,10] Incubation with O_2 under electron-poor conditions favors formation of the "unready" or Ni_u-A state for which reductive reactivation is much slower. The bridging ligand in the Ni_u-A state is likely to be a partially reduced form of O_2, probably a hydroperoxide.[5–7,11] Some

[a] Institut für Biologie/Mikrobiologie, Humboldt-Universität zu Berlin,
Chausseestr. 117, 10115 Berlin, Germany
[b] Inorganic Chemistry Laboratory, Department of Chemistry, University of Oxford,
South Parks Road, Oxford, OX1 3QR, United Kingdom
[c] Institut für Chemie, Sekr. PC14, Technische Universität Berlin, Straße des 17. Juni 135, 10623 Berlin, Germany
Fax: +49-30-31421122
E-mail: ingo.zebger@tu-berlin.de
[d] Institut für Physik, Freie Universität Berlin, Arnimallee 14, 14195 Berlin, Germany
[‡] These authors contributed equally to the work.
Supporting information for this article is available on the WWW under http://dx.doi.org/10.1002/ejic.201001053.

[NiFe] hydrogenases are able to catalyze hydrogen cycling even in the presence of O_2 (defined as "O_2-tolerance"),[12–14] making them attractive candidates for biotechnological applications such as enzymatic fuel cells or light driven H_2 production.[15,16] Here we focus on one prominent member of O_2-tolerant hydrogenases, namely the NAD^+-reducing soluble [NiFe] hydrogenase (SH) from *Ralstonia eutropha* H16, which belongs to the subclass of "bidirectional" hydrogenases. The SH directly couples H_2 oxidation with NAD^+ reduction in the presence of oxygen and provides the cells with reductants in the form of NADH.[17,18] This complex enzyme consists of two independent catalytic moieties: a heterodimeric hydrogenase module (subunits HoxH and HoxY) and a NADH:acceptor oxido-reductase (diaphorase) module consisting of HoxF and HoxU. The diaphorase module is very similar to the most peripheral solvent-exposed subunits of respiratory Complex I that harbor the NADH binding site. Two copies of the HoxI protein are further constituents of the SH; they are primarily attached to the HoxFU module and are proposed to provide an NADPH binding site.[19] In the SH holoenzyme, the NiFe catalytic center of the hydrogenase module is connected to the NAD^+-binding site of HoxF by a series of iron-sulfur clusters and two flavin mononucleotides, Figure 1.[20] One of the flavin units, designated as FMN-b, is a constituent of the HoxFU module, whereas the second flavin, FMN-a, has been suggested to be bound to the hydrogenase small subunit HoxY.[21] This assignment was based on the observation that the N-terminal region of HoxY is very similar to the FMN-binding region of flavodoxin.[22] Van der Linden and coworkers have found that FMN-a is loosely bound to the protein and can be easily released upon reduction with NADH.[21]

It was previously suggested that the O_2 tolerance of the SH is related to a modified catalytic site with two additional cyanide ligands compared to standard [NiFe] hydrogenases.[24–26] However, in a recent in situ EPR and FTIR spectroscopic study, it was demonstrated that the SH within living cells has a standard set of inorganic ligands, i.e., one CO and two CN^- ligands (Figure 1, enlargement).[23] The molecular mechanism underlying the O_2-tolerance of the SH is still unclear.

Because of the high complexity of the SH regarding subunit and cofactor content, it is desirable to investigate the individual catalytic modules independently in order to break the reaction mechanism of the SH into manageable parts. In an earlier study, the HoxHY moiety of *Rhodococcus opacus* SH, which is very similar to that of *R. eutropha*,[27,28] was investigated independently from the HoxFU module to examine its function and EPR spectroscopic properties. The *Rhodococcus opacus* protein is active in both H_2 production and oxidation[28] and its isolated hydrogenase module displays a prominent EPR signal at $g = 2.01$ under oxidizing conditions. This was interpreted as corresponding to a high potential $[4Fe4S]^{3+}$ or a $[3Fe4S]^+$ species as no EPR signal was detected in the reduced protein.[27]

Here we present the construction, purification, and biochemical, spectroscopic and electrochemical characterization of the smallest enzymatically active hydrogenase moiety of the SH from *R. eutropha*. In contrast to the *Rhodococcus opacus* HoxHY hydrogenase module, which can be easily separated from the corresponding diaphorase moiety just by exclusion of divalent metal ions (Ni^{2+}, Co^{2+}, Mg^{2+}, Mn^{2+}) and by decreasing the ionic strength of the buffer,[28] the corresponding hydrogenase module from the *R. eutropha* SH was generated by genetic engineering. Biochemical and direct electrochemical methods in combination with FTIR and XAS spectroscopy allowed the assignment of cofactors in the HoxHY subunits, evaluation of the catalytic activity of the hydrogenase module for H^+ reduction and H_2 oxidation, and analysis of potential dependent activation and inactivation reactions. The results are discussed in the context of the behavior of other O_2-tolerant hydrogenases and the related bidirectional hydrogenases from the actinomycete *R. opacus* and the cyanobacterium *Synechocystis* sp. PCC 6803.

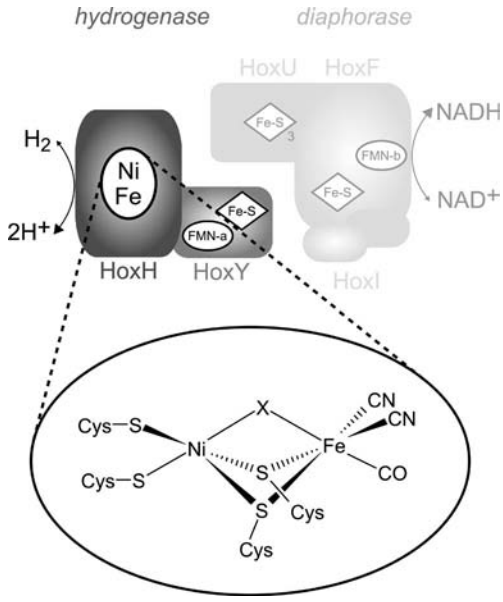

Figure 1. Schematic model of the soluble, NAD^+-reducing [NiFe] hydrogenase from *R. eutropha* and the proposed arrangement of redox cofactors. The enzyme consists of the heterodimeric hydrogenase module (HoxHY), investigated in this study, and a diaphorase module comprising HoxFU. Furthermore, two HoxI subunits are associated to the SH. The enlargement shows the active site structure of the SH hydrogenase module, which has recently been shown to harbor one CO and two CN^- ligands, analogous to O_2-sensitive "standard" [NiFe] hydrogenases.[22,23] The nature of the bridging ligand X depends on the redox state (see text).

Results and Discussion

Purification and Biochemical Characterization of HoxHY

For the purification of the SH hydrogenase moiety, consisting of the HoxH and HoxY subunits, we employed a plasmid derivative originally harboring the *hoxFUYHWIhypA2B2F2CDEX* genes. The genes *hoxF* and *hoxU* encoding the NADH:acceptor oxidoreductase module of

the SH were deleted from this plasmid. Additionally, the 5′ end of the *hoxY* gene was equipped with a sequence that codes for the *Strep*-tag II peptide. The resulting expression plasmid was maintained in *R. eutropha* HF788 lacking the megaplasmid pHG1, which encodes all hydrogenases known in *R. eutropha*.

Due to the missing HoxFU module, *R. eutropha* HF788 was unable to grow on H_2 and CO_2 as the sole energy and carbon sources. The strain was therefore cultivated heterotrophically under hydrogenase-derepressing conditions leading to the synthesis of the HoxHY module, which was purified to homogeneity by *Strep*-Tactin affinity chromatography. SDS-PAGE in conjunction with immunological analysis (Figure 2) revealed two protein bands assigned to HoxH and HoxY. From 32 g (wet weight) of cells, we routinely obtained 1.2 mg of HoxHY with an apparent molecular mass of 67 kDa and a specific H_2-evolving activity of 10–12 Units/mg of protein using reduced methyl viologen (MV) as the electron donor. Notably, the H_2-evolving activity was not enhanced by anaerobic purification of HoxHY or by the addition of FMN (data not shown).

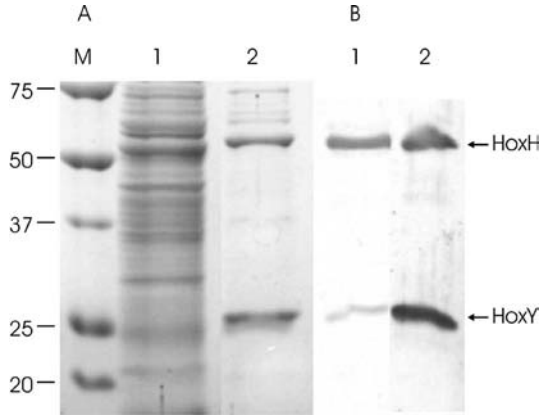

Figure 2. Purification of the HoxHY module of the *R. eutropha* SH: 30 μg of soluble extract (1) and 3 μg of purified HoxHY (2) were electrophoretically separated on an 12% SDS-polyacrylamide gel and subsequently stained with Coomassie brilliant blue (A). Panel B shows the immunological detection of HoxH and HoxY using specific antibodies. Lane M displays marker proteins and their corresponding molecular weight in kDa.

HoxHY showed H_2-oxidizing activity in solution assays only after pre-incubation with dithionite indicating that the as-isolated protein requires reductive reactivation (Table 1). In native SH, this reductive reactivation is accomplished by the physiological reductant NADH.[18] Upon addition of FMN to the assay, we observed a 3–4 fold increase in H_2 oxidation activity suggesting that FMN facilitates electron transport (Table 1).

The UV/Vis spectrum for HoxHY reduced with 0.1 mM sodium dithionite (DT) shows prominent peaks at 382 nm and 394 nm (Figure 3), which are characteristic of an anionic semiquinone radical, whereas the shoulders at 551 nm and 600 nm are indicative of a neutral semiquinone radical.[29] A corresponding FMN fluorescence determination, however, revealed only 0.05 equiv. of FMN per HoxHY

Table 1. H_2 oxidation activity of HoxHY.[a] Values represent the arithmetic means and standard deviations of three independent experiments.

Assay conditions	H_2-dependent reduction of MV [Units/mg]
Without pre-incubation	< 0.05
Pre-incubation with DT	1.02 ± 0.14
Pre-incubation with DT and FMN	3.75 ± 0.49

[a] Details are given in the experimental section.

unit. The substoichiometric amounts may be due to the absence of the HoxFU module, which probably contributes to FMN-a binding. Flavin can act as a communicator between intramolecular one-electron centers (e.g. iron sulfur clusters) and two-electron transferring cofactors (e.g. NADH) as described for many flavometalloenzymes.[30,31] Van der Linden and coworkers proposed that FMN-a in HoxHY functions as a two-to-one electron converter between the hydride formed during catalysis at the [NiFe] active site and the Fe-S clusters.[21]

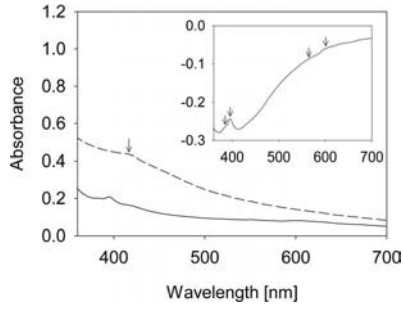

Figure 3. UV/Vis spectra of the oxidized (ox., dashed line) and dithionite-reduced HoxHY (red., solid line). The protein concentration was 4.5 mg/mL. The inset shows the corresponding difference spectrum (red. – ox.) with peaks and shoulders indicated by arrows (see text for assignment).

Additionally, it is possible that the FMN-a is part of the electron transport chain that enables (fast) removal of oxygen species from the inactivated [NiFe] catalytic center.

Metal determination by total reflection X-ray fluorescence (TXRF) resulted in the detection of Ni, Fe, Cr, Cu, and Zn in a ratio of 1:6.2:0.3:1.4:0.4, which supports the presence of one [4Fe4S] cluster in HoxY in addition to the active-site iron atom in HoxH. The detection of copper in the HoxHY module is in agreement with the previous finding of 0.63 copper atoms in the related SH hydrogenase module isolated from *Rhodococcus opacus*.[27] The binding of Cu, Cr, and Zn is assumed to be nonspecific and may be related to the exposure of metal-binding amino acids as a result of the removal of the HoxFU moiety. Indeed, in addition to the four proposed [4Fe4S] cluster-coordinating cysteines, HoxY contains five extra cysteine and five histidine residues (Figure S1). The presence of an Fe-S cluster is further supported by the UV/Vis absorption spectrum of as-isolated oxidized HoxHY (Figure 3) showing a very broad absorption between 350 and 500 nm with a shoulder at 415 nm that is typical for Fe-S cluster-containing proteins. EPR analysis of as-isolated HoxHY at temperatures

between 10 and 80 K revealed no signals from either the [NiFe] site or the iron sulfur cluster of HoxHY. Also no EPR signals were observed after treatment with dithionite or H_2 (data not shown).

X-ray Absorption Spectroscopy (XAS)

The nature of the Fe-S cluster in the as-isolated HoxHY moiety was studied using XAS. The Fe *K*-edge differed from spectra of iron complexes with only sulfur coordination[33] in that its primary maximum exceeded unity absorption and the pre-edge feature at ca. 7113 eV due to $1s \rightarrow 3d$ electronic transitions was relatively weak (Figure 4). The edge shape was more similar to spectra of, for example, [FeFe] hydrogenase showing contributions from both Fe–S and Fe–C(=O/N) interactions in the H-cluster.[3,34] This result was in agreement with the presence of the C(=O/N)- and sulfur-coordinated active-site Fe, an Fe-S cluster, and possibly of further oxygen-ligated Fe in the HoxHY preparation. A best-fit simulation of the EXAFS spectrum revealed relatively large contributions from short Fe–C(=O/N) bonds (1.84 Å) to the EXAFS (Table 2). The coordination number of the Fe–C(=O/N) interactions (ca. 0.7) was close to that of ca. 0.5 expected for an active-site Fe coordinated by three diatomic ligands and ca. 6 Fe ions in the sample. Simulation revealed three different metal–metal distances. The shortest intermetal distance was attributed to the Ni–Fe distance. About two Fe–Fe distances per iron of ca. 2.7 Å were detected, typical for normal Fe-S clusters.[34] For the presence of the active-site iron and a [2Fe2S], [3Fe4S], or [4Fe4S] cluster, $N_{2.7}$-values of about 0.7, 1.5, or 2.4 were expected. The EXAFS analysis also revealed a low amount of metal–metal distances of ca. 3.3 Å and Fe–O bonds of 2.14 Å (Table 2), possibly stemming from Fe–O–Fe motifs, which may be due to oxidatively modified Fe-S clusters[33] and/or nonspecific iron in the sample. The latter also was suggested by the average Fe:Ni ratio of ca. 6:1.

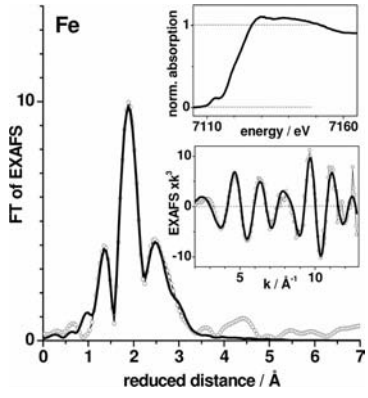

Figure 4. Iron XAS analysis of HoxHY. The Fourier-transform (FT) of the EXAFS oscillations in the lower inset shows peaks due to Fe–C(=O/N), Fe–S/O, and Fe–Fe/Ni distances. Experimental data, open circles; EXAFS simulation with parameters in Table 2, solid line. The FT was calculated using $\cos^2$ windows extending over 10% at both *k*-range ends. The corresponding *K*-edge spectrum is shown in the upper inset.

Such contributions diminished the apparent $N_{2.7}$ value, which thus was compatible with that expected for a [4Fe4S] cluster. The coordination number of the Fe–S interactions of about 3.2 (Table 2) was in reasonable agreement with the value of ca. 3.3, which was calculated for two Fe–S bonds at the active site, a [4Fe4S] cluster, and ca. 6 Fe atoms in the sample. Thus, EXAFS analysis in combination with the metal content determined by TXRF and the conserved cysteines (Figure S1 in the Supporting Information) suggest the binding of a [4Fe4S] cluster in HoxHY in the dominant protein fraction. In a minor proportion of the sample, this cluster may have been converted into a [4Fe-nS-nO] species by oxidative modification.[33]

Table 2. EXAFS simulation parameters. N_i, coordination number; R_i, metal-backscatterer distance; $2\sigma^2_i$, Debye–Waller parameter. The fit error, R_F[32] as calculated over reduced distances of 1–3 Å was 9.5%.

Shell	N_i (per metal)	R_i [Å]	$2\sigma^2_i$ [Å^2]
C(=O/N)	0.74[a]	1.84	0.002[b]
O	1.05[a]	2.14	0.002
S	3.21[a]	2.24	0.007[b]
Ni	0.64	2.52	0.002[b]
Fe	2.11	2.70	0.005[b]
(C=)O/N_{ms}	0.74	2.98	0.005[b]
Fe	0.68	3.38	0.005[b]

[a] The sum of the first-sphere coordination numbers was restricted to 5. [b] Parameters that were fixed to physically reasonable values in the simulations; the coordination number of multiple-scattering (ms) contributions of (C=)O/N ligands was set to that of the Fe–C(=O/N) bonds.

Electrochemistry

We carried out direct electrochemical experiments on a film of HoxHY adsorbed on a pyrolytic graphite edge (PGE) electrode to examine electrocatalytic activity and reactions with inhibitors/inactivators. Figure 5 shows cyclic voltammograms recorded in H_2-equilibrated buffer at pH 6.0, 7.0, and 8.0 for a film of HoxHY, which confirm that the enzyme moiety is able to oxidize H_2 and reduce H^+ after an activation process. The response at an unmodified PGE electrode under analogous conditions is also shown in each panel since the background capacitive current is significant in comparison to the fairly low electrocatalytic current associated with the hydrogenase heterodimer. The electrode was stationary during these experiments to avoid destabilisation of the protein film, but in the scan in panel C, the electrode was rotated for a brief period on the return sweep (indicated by an asterisk *) to confirm that the current is not limited by mass transport of H_2. Voltammograms in panels A–C were recorded at a fairly slow scan rate (1 mV/s) and initiated from 0 V vs. SHE in order to examine the reductive activation of the as-isolated enzyme. The scan shown in panel A was recorded at pH 8.0, and at the commencement of the sweep, the current remains close to zero, since as-isolated HoxHY is inactive for H_2 oxidation. The current begins to rise at approximately –0.3 V, just positive of the potential for $E(2H^+/H_2)$, corrected for the experimental

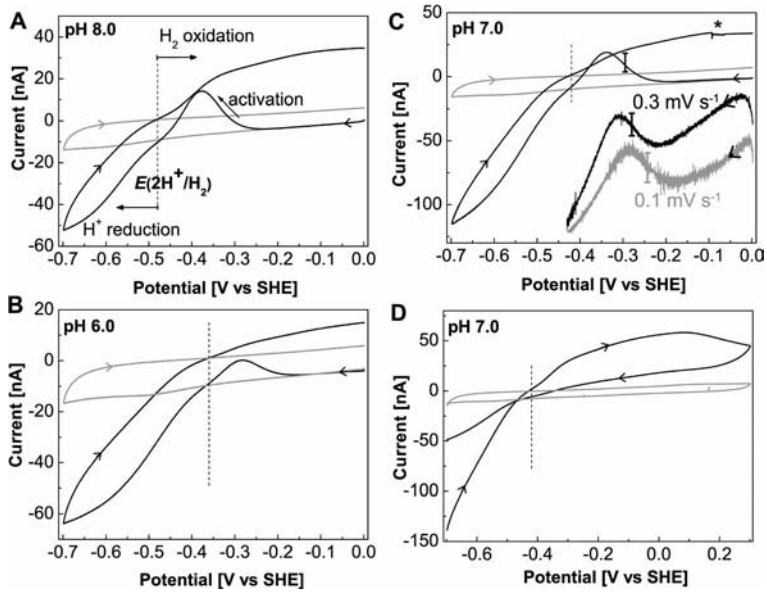

Figure 5. Cyclic voltammograms recorded at 1 mV/s for as-isolated HoxHY on a PGE electrode in potassium phosphate buffer (50 mM) at the pH values indicated at 30 °C, 1 bar H_2. Scans A–C were initiated from 0 V vs. SHE after 20 s equilibration at this potential. The position of $E(2H^+/H_2)$, corrected for experimental conditions, is shown as a dashed vertical line on each panel and the response at an unmodified PGE electrode under analogous conditions is shown as a gray line. On the voltammogram in panel C, the electrode was rotated for a brief period, indicated by *, to confirm that the current is not limited by H_2 mass transport. Also plotted in panel C are linear sweep voltammograms for as-isolated HoxHY recorded at different scan rates; due to loss of protein film during the very slow sweeps, the current is magnified × 100 and for clarity is offset on the vertical axis. Switch-on potentials [E_{switch} (1 mV/s); see text] are indicated as vertical bars. Panel D shows a voltammogram recorded after a preactivation sweep to low potentials. The direction of each scan is indicated by arrowheads.

conditions (–0.48 V, vertical dashed line) as the as-isolated enzyme moiety is activated and H_2 oxidation is switched on. This is consistent with the requirement for low potential reductants for activation of HoxHY in solution assays, and confirms that the presence of H_2 alone is not sufficient to activate HoxHY. The current drops as the driving force for H_2 oxidation diminishes, and then becomes negative as H^+ reduction by immobilised HoxHY commences at potentials more negative than $E(2H^+/H_2)$. On the return sweep, a catalytic wave consistent with H_2 oxidation is evident at potentials more positive than $E(2H^+/H_2)$. On the second cycle the reactivation peak is absent (not shown), confirming that the as-isolated enzyme requires a single reductive activation step.

Since the catalytic current is directly proportional to electrocatalytic activity at any given potential, the H^+ reduction current relative to H_2 oxidation current for each return sweep in Figure 5 provides a measure of the catalytic bias of HoxHY at the respective pH. Physiologically relevant potentials for operation of HoxHY within the intact soluble hydrogenase are likely to lie within the range $E(2H^+/H_2) \pm 150$ mV. At pH 8.0 and 1 bar H_2, the H^+ reduction activity at 150 mV below $E(2H^+/H_2)$ is just 1.2 times the H_2 oxidation activity measured at 150 mV above $E(2H^+/H_2)$. As expected, the relative H^+ reduction rate increases with availability of protons: at pH 6.0 and pH 7.0 and 1 bar H_2, the H^+ reduction rate is approximately twice the H_2 oxidation rate. Thus, the hydrogenase module of the SH is equipped to work in either direction.

Voltammograms recorded at pH 7.0 at slower scan rates (Figure 5, panel C) show that the position of the activation peak for as-isolated HoxHY shifts to more positive values as the potential is scanned more slowly. Due to the instability of HoxHY films on the electrode we were unable to record scans slower than 0.1 mV/s to see whether the activation tends towards a particular potential, and the switch-on potentials evident in Figure 5 therefore represent convoluted thermodynamic and kinetic contributions. A parameter, E_{switch}, has previously been used to describe the reactivation of [NiFe] hydrogenases and defined as the potential (E) of steepest current (i) ascent during activation (minimum in di/dE), noting that the scan rate must be slow relative to the activation rate in order to record a meaningful potential.[4,35] Nevertheless, values of E_{switch} determined at a particular scan rate enable comparison of the effects of different conditions and of the behavior of different hydrogenases.[36] The observation that the activation of as-isolated HoxHY in the H_2 oxidation region is slow even at extremely negative potentials (close to the onset of H^+ reduction) is informative: a low potential reductant would be required to restore activity to HoxHY in this state. This should be available in vivo from the NAD^+/NADH pool which is coupled to HoxHY by the HoxFU subunits of the SH.[18,19] For as-isolated HoxHY, E_{switch} (1 mV/s) at pH 8.0, 7.0, and 6.0 is –340 , –300, and –245 mV, respectively, confirming that reductive reactivation is coupled to proton transfer. In contrast, the inactive state of the MBH of *R. eutropha* shows a much more positive value for E_{switch},

+115 mV vs. SHE at pH 6.0, 30 °C at 1 mV/s, consistent with the fact that it is coupled to the higher potential periplasmic membrane quinone pool.[37] Both Hyd-1 and Hyd-2 from *E. coli* also have E_{switch} values significantly more positive than as-isolated HoxHY when examined under identical conditions (+150 and –85 mV, respectively, at pH 6.0).[13]

Under anaerobic conditions, most [NiFe] hydrogenases show a characteristic reversible switch-off in activity at high potentials corresponding to generation of the inactive Ni_r-B state.[4,37] Panel D of Figure 5 shows a slow scan for HoxHY in which the potential was swept at 1 mV/s from –700 to 300 mV. Above 0 V, the activity drops off, but no corresponding reductive reactivation is observed on the slow return sweep suggesting that HoxHY does not form a conventional Ni_r-B state. Loss of activity at high potential thus appears to be irreversible and may be due to potential-dependent film loss or protein damage.

We examined the H^+ reduction reaction of HoxHY to determine whether this is inhibited by the product, H_2. The experiment shown in Figure 6 was carried out at 10 °C to take advantage of the improved stability of HoxHY on the electrode at lower temperatures over the extended time periods required for gas exchange steps. The data reveal that H_2 production by HoxHY is inhibited by H_2, as observed for many [NiFe] hydrogenases. The MBH from *R. eutropha* is so strongly inhibited by H_2 that H^+ reduction is barely detectable under a H_2 atmosphere.[37] Inhibition is evidently weaker for HoxHY, with ca. 30–40% of H^+ reduction activity retained under 100% H_2, in line with the role of the SH as a bidirectional enzyme in vivo.

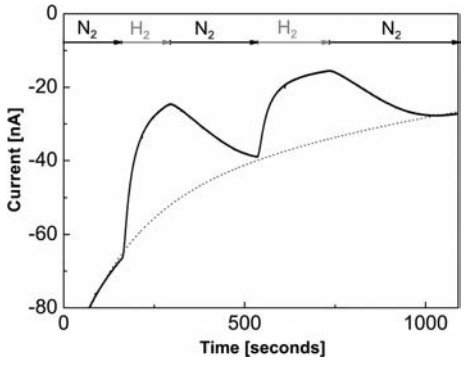

Figure 6. Experiment designed to examine inhibition of H^+ reduction by H_2 (product inhibition). The gas flushing through the headspace of the cell was exchanged at the times indicated maintaining an overall flow rate of 1 L/min. The dotted line indicates an exponential fit to the background decay in current during periods in which the cell is equilibrated with N_2, attributed to film loss. Other conditions: 10 °C, pH 7.0, electrode rotation rate: 2000 rpm, electrode potential: –584 mV.

Protein film electrochemistry was applied to investigate the effects of O_2 on HoxHY (Figure 7). The experiment shown as a black solid line in panel A was again carried out at 10 °C. The HoxHY film was first reductively activated, and then the electrode was poised at a potential sufficiently high to avoid direct reduction of O_2 at graphite, 216 mV. At 90 s, 2% O_2 was introduced, causing the H_2 oxidation activity of HoxHY to decay slowly almost to zero. Data from time points beyond the first 35 s fit well to a single exponential function as shown in the semilogarithmic plot inset A in Figure 7 (black line and grey dashed fit), yielding a first-order rate constant of 0.01 s^{-1} at 10 °C, pH 7.0, 2% O_2. For data recorded at 30 °C (part A of Figure 7, dotted line in main panel and inset), inactivation is complicated by poorer film stability, but the semilogarithmic plot confirms that inactivation by O_2 is approximately twice as fast at this temperature (deviation from first order kinetics at early time points is likely to be due to incomplete gas mixing). After removing O_2 by flushing with 98% H_2, 2% N_2, three successively longer reductive steps were applied (to –384 mV). The current at 216 mV following each reductive poise (after decay of the capacitive current associated with the potential jump) provides a measure of the extent of reactivation induced by the step to –384 mV. The first 10 s reductive step induces a substantial recovery of the current at 216 mV, and two further reductive steps induce no further increase in current. A first order exponential function fitted to the "film loss" curve in the first 90 s before introduction of O_2 (dashed black line) can be extrapolated to the current level reached at 216 mV after reductive activation, suggesting that activity may be fully recovered. For comparison, a control experiment performed under anaerobic conditions is also shown in Figure 7 (A) along with a corresponding exponential "film loss" decay curve (solid and dashed gray lines, respectively).

Part B of Figure 7 shows results, which confirm that the O_2 inactivated state of HoxHY reactivates rapidly at –384 mV even in the presence of 2% O_2. Preactivated HoxHY was first poised at 216 mV under H_2, and 2% O_2 was introduced at 90 s (i) as in (A). After inactivation by O_2, brief reductive poises were then applied with continual flushing of 2% O_2:98% H_2 through the headspace. The potential was returned to 216 mV at (ii) and (iii) to monitor HoxHY activity. Interpretation of the current at (ii) and (iii) is complicated. Decay of capacitive current ensuing from the potential step gives a background contribution, as shown for the control experiment on a "dead" film of HoxHY (thin black line). The gray trace represents a subtraction of this current from the thick black trace to give an indication of the contribution of HoxHY electrocatalysis to the overall current. Capacitance is not identical between the electrode preparations, but it is clear that HoxHY activity has been restored by the brief *aerobic* reductive poise. The electrocatalytic current then decays again as HoxHY is inactivated by O_2. In the final stage of the experiment, 2% N_2:98% H_2 was flushed through the headspace to remove O_2. The dashed line represents a possible fit to an exponential decay of current due to film loss throughout the experiment. We are unable to directly measure H_2 oxidation by HoxHY under aerobic conditions at potentials close to the NAD^+/NADH potential due to significant reduction of O_2 at graphite below 0 V. However, the set of experiments shown in Figure 7 (B) provides indirect evidence that HoxHY is able to attain full activity at –384 mV

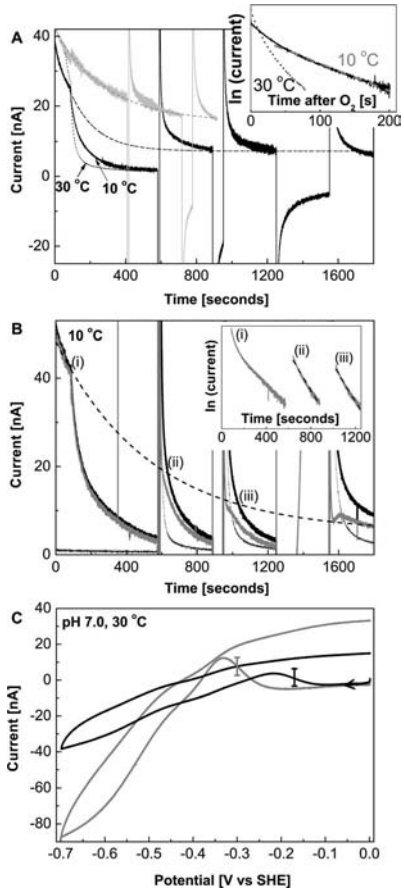

Figure 7. Experiments designed to monitor reaction of HoxHY with O_2 and the rate and extent of reductive reactivation under anaerobic and aerobic conditions. Panel A: Thick black line: current-time trace recorded at 10 °C in which HoxHY was first reductively activated, and then the electrode was poised at 216 mV with 98% H_2:2% N_2 flushing through the cell headspace. At 90 s, an aliquot of O_2-saturated buffer was injected into the cell to bring the solution concentration instantaneously to 2% O_2, and simultaneously, the gas flow in the headspace was exchanged for 98% H_2:2% O_2. At 250 s, the cell was flushed with 98% H_2:2% N_2 again. Reductive poises were then applied, returning to 216 mV after each: 580 s: 10 s at –384 mV; 890 s: 60 s at –384 mV; 1250 s: 300 s at –384 mV. Data showing the effect of an analogous O_2 introduction at 30 °C are shown as a dotted black line. The thick gray line shows a control trace performed at 10 °C under fully anaerobic conditions with 98% H_2:2% N_2 as the headgas; at 90 s, an aliquot of N_2-saturated buffer was injected to confirm that an injection does not perturb the current and reductive poises were then applied: 410 s: 10 s –384 mV; 715 s: 60 s at –384 mV. Dashed black and gray lines show an extrapolation to an exponential fit to the background current decay attributed to film loss. Inset in (A) is shown a semilogarithmic plot for the decay in current following introduction of O_2. Panel B: Thick black line: current-time trace in which HoxHY was first reductively activated, and then the electrode was poised at 216 mV with 98% H_2:2% N_2 flushing through the cell headspace. At 90 s (i), 2% O_2 was introduced and kept at this level until the final section of the experiment at 1550 s. Reductive poises were applied, returning to 216 mV after each [(ii) and (iii)]: 580 s: 10 s at –384 mV; 890 s: 60 s at –384 mV; 1250 s: 300 s at –384 mV. The thin black line shows a control trace for a "dead" HoxHY film under the same conditions as the thick black line. The gray line represents subtraction of the thin black trace from the thick black trace. Inset in panel B is shown a semilogarithmic plot for the decay in current following introduction of O_2 at (i), (ii), and (iii). All experiments in panels A and B were recorded with the electrode rotating at 2000 rpm and with an overall gas flow rate of 1 L/min. Panel C: cyclic voltammogram (black line) recorded at 1 mV/s, 30 °C and pH 7.0 at a stationary electrode after exposure of pre-activated HoxHY to O_2 (2% at 10 °C) and subsequent removal of O_2 from the cell by gas exchange. The gray line reproduces the trace from Figure 5 (C) for comparison. Switch potentials (1 mV/s) determined from derivative plots (not shown) are marked by vertical bars.

in the presence of 2% O_2, which would enable O_2-tolerant H_2 oxidation by HoxHY at physiologically relevant potentials.

Part C of Figure 7 shows a similar experiment in which HoxHY was first inactivated by O_2 at 10 °C, and then after raising the temperature to 30 °C and flushing out the O_2, the potential was swept slowly towards more negative values to monitor the potential dependence of reactivation. HoxHY then shows a reductive reactivation switch-on at –170 mV, indicating that O_2 reaction at 216 mV generates an inactive state that is distinct from the as-isolated state which reactivates at about –300 mV under identical conditions.

In vivo the SH couples NAD^+ reduction to H_2 oxidation in the presence of O_2, although the physiological levels of O_2 in the cytoplasm are not known accurately. The electrochemical results show that HoxHY has a half life of about 1 min at 10 °C, 216 mV, and 2% O_2, but that activity is recovered rapidly at lower potentials (complete within the timeframe of a 10 s step to –384 mV), even in the presence of O_2. The value of –170 mV for E_{switch} (1 mV/s, 30 °C, pH 7.0) measured for the O_2-inactivated HoxHY species suggests that in the intact SH in which HoxHY is coupled to the NAD^+/NADH potential, recovery should be fast relative to inactivation by O_2, allowing the enzyme to continue oxidizing H_2 under aerobic conditions at potentials close to $E(2H^+/H_2)$. The rate of reaction with O_2 at 30 °C, 216 mV, and 2% O_2 (approximately 0.02 s^{-1}) is slow compared with rates measured for the O_2-sensitive wild type [NiFe] hydrogenase from *Desulfovibrio fructosovorans* (ca. 0.8 s^{-1} under similar conditions), or even variants of this enzyme with impaired gas access (0.1 s^{-1} for a V74Q mutant).[38] It is also slow compared to O_2 inactivation rates measured for several [FeFe] hydrogenases,[38] although similar to that measured for the *Clamydomonas reinhardtii* enzyme. The O_2-tolerant [NiFe] membrane-bound hydrogenase from *Aquifex aeolicus* has also been found to react slowly with O_2,[14] and a slow rate of O_2 access in HoxHY may contribute to protection of the SH during aerobic operation.

FTIR Spectroscopy

FTIR data for different isolated samples of HoxHY are presented as baseline-corrected absorption spectra in Figure 8 (left and center panel). For a more precise identification of ν(CO) and ν(CN) band positions, second derivatives of the untreated spectra were taken into consideration (Figure S2), as they show distinct negative peaks for individual absorption bands. In order to cope with intrinsically low band intensities of the diatomic ligands and strong baseline effects, in vivo spectra for HoxHY within living cells are exclusively plotted as second derivatives in the right hand panel of Figure 8.

The active site of the purified, as-isolated HoxHY protein exhibits two redox states, denoted here as Ni-Ox and Ni-Ox2, which appear in varying amounts (see also Figure S3). For a closer investigation of their individual character-

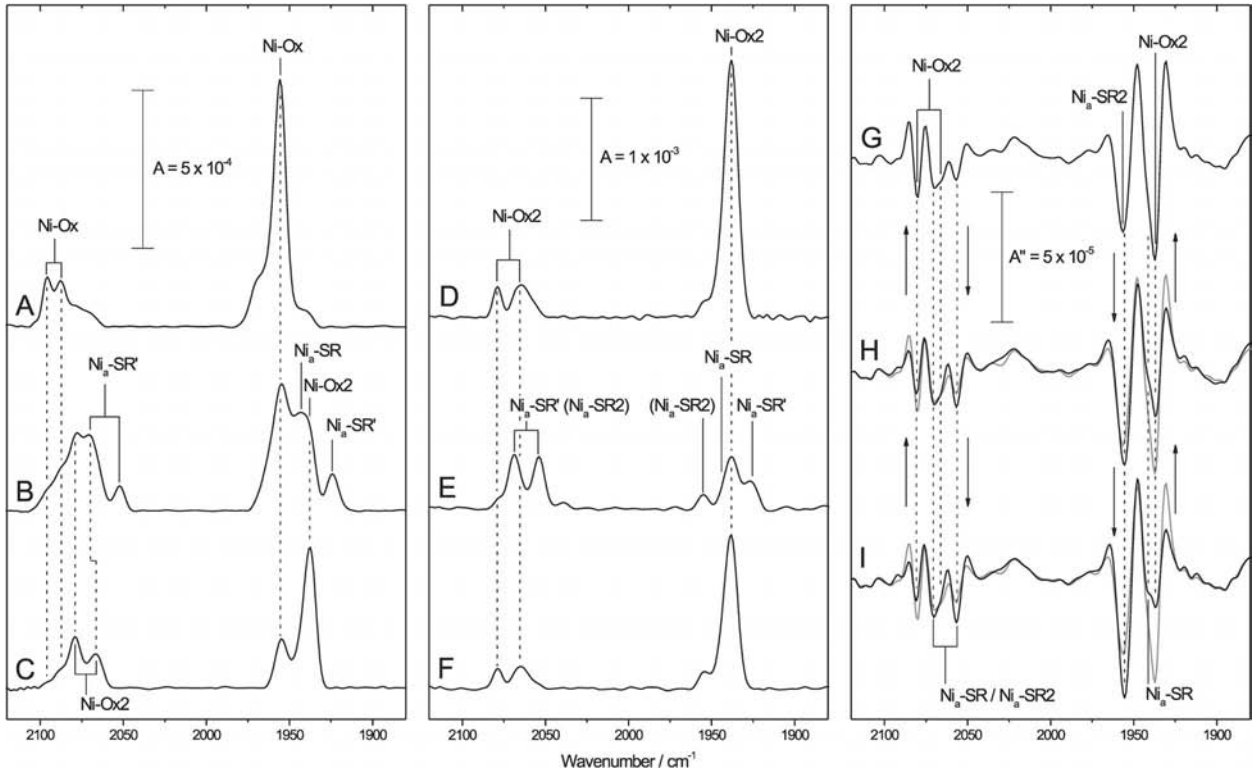

Figure 8. FTIR spectra of the *R. eutropha* HoxHY, recorded at 10 °C, traces A–F are displayed as absorbance spectra (*A*). Left hand panel: A: as-isolated in the Ni-Ox state; B: after reductive activation of the sample from (A) with 1 bar H_2 in the presence of FMN; C: after partial reoxidation of the sample from (B) by slow influx of O_2. Central panel: D: as-isolated HoxHY from a different preparation showing predominantly the Ni-OX_2 state; E: after reductive activation of the sample from (D) with 1 bar H_2 in the presence of FMN; F: after partial reoxidation of the sample from (E) by slow influx of O_2. Right hand panel: in vivo FTIR spectra of HoxHY (second derivatives, *A''*): after five (G), six (H), and seven days (I) of cultivation, respectively.

istics, HoxHY preparations with predominant contributions from Ni-Ox or Ni-Ox2, respectively, are discussed below. The left hand panel of Figure 8 shows results for a typical sample of as-isolated HoxHY, which initially resides largely in an oxidized state, characterized by one ν(CO) and two ν(CN) bands at 1956 and 2087/2096 cm^{-1}, respectively (Figure 8, A). The band pattern confirms that the [NiFe] active site in HoxHY comprises a standard set of inorganic ligands, i.e., one CO and two CN^- ligands, as reported for the native SH in whole cells.[23] The position of the ν(CO) and ν(CN) absorption bands resemble those of the unready Ni_u-A state of standard [NiFe] hydrogenases, such as the enzyme from *D. vulgaris* Miyazaki F,[39] indicating a highly oxidized species. In the case of HoxHY, however, the observed state appears to be EPR silent (not shown). Consequently, this species is assigned to a novel oxidized state, termed Ni-Ox (oxidized). Two additional ν(CN) bands at 2069 and 2079 cm^{-1} show up to indicate a further, oxidized (sub-) species, which, however, appears to be degenerate with respect to the CO stretching vibration. Shoulders on either side of the ν(CO) band do not correlate with the appearance and/or relative intensity of any of the ν(CN) absorptions and are therefore attributed to minor subfractions of HoxHY of unknown structure. The presence of atmospheric O_2, FMN, or tris(2-carboxyethyl)phosphane (TECP) did not induce any changes in the Ni-Ox state of as-isolated HoxHY (not shown).

Spectra in the central panel of Figure 8 were recorded for a HoxHY preparation that was found to reside predominantly in a different oxidized redox state characterized by one ν(CO) and two ν(CN) bands at 1938 and 2065/2079 cm^{-1}, respectively (Figure 8, D). The observed species, denoted as Ni-Ox2, appears to be EPR silent, too. This state also arose upon reduction of the Ni-Ox state with H_2, a reaction which was partially reversible upon reoxidation with O_2 (Figure S4). This, together with the lower CO and CN stretching mode frequencies, suggests that Ni-Ox2 is a less oxidized, though still inactive species. The addition of FMN and/or dithiothreitol (DTT) had no effect on the FTIR spectrum of purified HoxHY residing in the Ni-Ox2 state. Notably, the Ni-Ox2 species was not observed at significant levels in preparations of the native SH within cells.[23] Its formation is therefore likely to be related to the absence of the stabilizing diaphorase moiety and/or a substoichiometric FMN content.

Spectroscopic investigations of SH residing in living cells have been shown to be valuable in reporting on the active site (electronic) structure, its redox states, and the behavior of the enzyme in its native environment.[23] We therefore also carried out in vivo spectroscopic studies on the

HoxHY moiety (Figure 8, G–I). In freshly harvested cells, HoxHY was found to adopt two major redox states, one of which is the Ni-Ox2 species, observed also for as-isolated enzyme, which is characterized by ν(CO) and ν(CN) bands at 1938 and 2065/2079 cm^{-1}, respectively. Minor deviations of the low-frequency CN stretching are due to an overlap with a nearby absorption, corresponding to HoxHY in another redox state (see below). The more oxidized Ni-Ox species was not detected in vivo, which is consistent with the reducing conditions within the cytoplasm. The second major redox state with corresponding ν(CO) and ν(CN) bands at 1956 cm^{-1} and 2057/2069 cm^{-1}, respectively, accumulated with increasing cell density during the cultivation process (Figure 8, G–I). Higher cell densities generally lead to O_2 limitation and a resultant increase in the cellular pool of reductants, which is in line with the concomitant accumulation of the state previously assigned as Ni_a-SR, indicated by an increasing shoulder at 1941 cm^{-1}.[23] Therefore, it is likely that the observed species represents a highly reduced state of HoxHY. On the basis of the high-frequency CO absorption band, this redox state is tentatively assigned to the reduced Ni_a-SR2 state, which was recently observed for the native SH from *R. eutropha* and the related "bidirectional" soluble [NiFe] hydrogenase from *Synechocystis sp.* PCC 6803.[23,40] Notable deviations in the ν(CN) band positions of the Ni_a-SR2 species might be related to the lack of the diaphorase moiety, the substoichiometric level of FMN, and resulting conformational and geometric changes at the active site. The absence of the reduced Ni_a-SR′ state, observed in vitro, can be explained by different pH values in the cytoplasm (close to pH 7) and the buffer of the purified enzyme (pH 8.0).

In further FTIR spectroscopic experiments, we investigated the activation of HoxHY isolated predominantly in the Ni-Ox and Ni-Ox2 state, respectively, and analyzed the resulting reduced forms. Purified HoxHY preparations in the Ni-Ox state can be activated by various artificial and native electron donors. However, in line with observations from spectrophotometric activity assays and electrochemistry no reduced states were observed upon incubation with pure H_2 in FTIR experiments (Figure S4). However, the simultaneous presence of FMN and H_2 revealed a substantial formation of reduced states (Figure 8, B), suggesting that the flavin cofactor is reincorporated under electron-rich conditions, as previously reported for the heterotetrameric SH (HoxHYFU).[21] In particular, generation of the Ni_a-SR′ species, (known for other [NiFe] hydrogenases) is indicated by ν(CO) and ν(CN) absorptions at 1923 and 2052/2069 cm^{-1}, respectively, whereas a further ν(CO) band at 1946 cm^{-1} suggests the concomitant appearance of the Ni_a-SR species.[23]

The Ni_a-SR2 state of HoxHY may also contribute to absorptions at 1956, 2052, and 2069 cm^{-1}. Bands at 1938, 2069, and 2079 cm^{-1} reflect a population trapped in the Ni-Ox2 state while residual fractions of Ni-Ox are indicated by absorption bands at 1956, 2088, and 2096 cm^{-1}. Remaining fractions of these two oxidized species may reflect HoxHY populations still lacking flavin. Alternatively, the incomplete activation of as-isolated HoxHY could be related to enzyme fractions with impaired electron transfer due to a modified Fe-S cluster as suggested by XAS.

Reduction of the Ni-Ox state of HoxHY was also observed in FTIR studies after incubation with artificial electron donors, such as dithionite or a mixture of dithionite and MV, both in the presence or absence of H_2 (Figure S5). This is in agreement with the findings from electrochemistry (see above and Figure S6) and in vitro H_2 production assays, that activation of HoxHY by artificial electron donors or an electrode does not necessarily require additional supply of FMN. These observations suggest a different activation mechanism and/or intramolecular electron pathway compared to activation by H_2, which was found to be dependent on FMN. However, with these treatments, the catalytically active species were formed at lower levels than under H_2/FMN reduction and larger amounts of the Ni-Ox2 state were induced. In the presence of FMN, slow exchange of H_2 against air (over ca. 11 h) resulted in a decrease in the concentration of all Ni_a-SR subspecies and an increase in the Ni-Ox2 population (Figure 8, C), suggesting partial reoxidation of HoxHY. Here, FMN was also found to contribute to the long-term stability of Ni-Ox2 (ca. 21 h), which otherwise degraded in the (prolonged) presence of pure H_2 (Figure S4).

Consistent with this observation, H_2 was also found to induce an extensive degradation of the active site in purified HoxHY residing in the Ni-Ox2 state, as indicated by a severe decrease of all CO and CN stretchings (not shown). Again, additional supply of FMN preserved the integrity of the active site, supporting the idea that FMN-a plays a stabilizing role and can be reincorporated. Furthermore, HoxHY was partially activated by H_2 in the presence of FMN, as indicated by Ni_a-SR′ absorptions at 1926, 2054, and 2069 cm^{-1} and a shoulder at 1944 cm^{-1} indicative of the Ni_a-SR state (Figure 8, E). Above-average intensity of the Ni_a-SR′ CN absorption bands and a 2 cm^{-1} shift of the corresponding low-frequency band towards higher wavenumbers suggests that the ν(CO) band at 1955 cm^{-1} might also have contributions from a Ni_a-SR2 fraction. A residual population of the Ni-Ox2 state is suggested by a strong ν(CO) band at 1938 cm^{-1}. The corresponding CN stretchings are, however, hardly detectable in the spectrum due to an overlap with other bands. After longer periods of time (ca. 21 h), slow O_2 diffusion into the IR cell induced oxidation of all reduced species and a repopulation of the Ni-Ox2 state, indicating the reversibility of the activation process (Figure 8, F).

The interconversions observed spectroscopically are summarized in Scheme 1, and an overview of the CO and CN stretching-mode frequencies for all states relative to those in native SH is given in Table 3. The most oxidized (inactive) state of HoxHY is Ni-Ox, while Ni-Ox2 appears to be an intermediate, yet inactive, species. Hence, the low potential activation step at –300 mV, observed in electrochemistry, is most likely related to the conversion of this redox state to the reduced, catalytically active Ni_a-SRX species. It is not yet clear how the activation step observed electro-

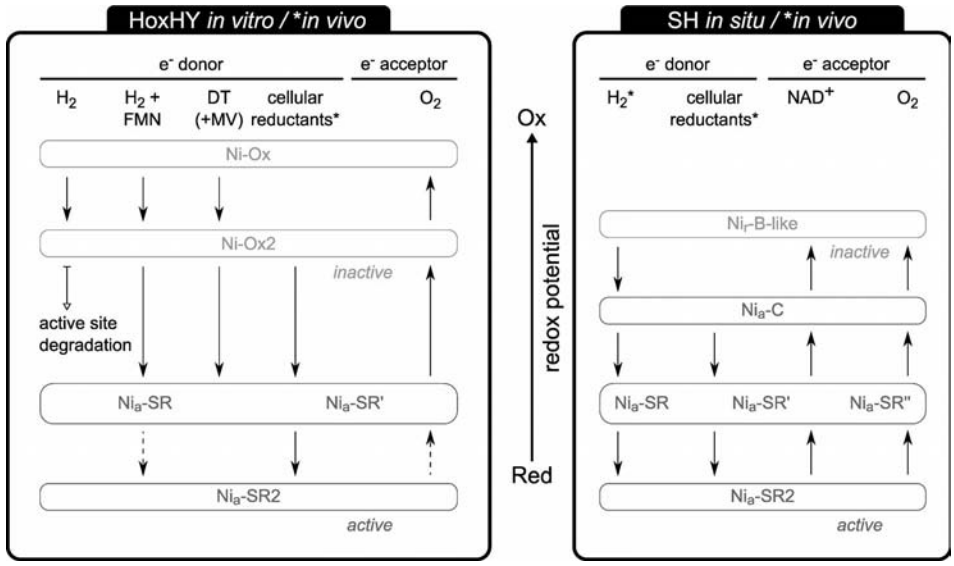

Scheme 1. Redox scheme for HoxHY and the native SH in whole cells, summarizing IR-detectable redox states and conversions under various conditions (see headings in line 2). Inactive and active species are displayed in light and dark grey, respectively. Tentative redox conversions are presented as dashed lines. Cellular reductants refer to cytoplasmic reducing equivalents which give rise to reduced HoxHY and native SH in whole cells, as observed by in vivo spectroscopy.[23]

chemically at –170 mV, after exposure of active enzyme to O_2, relates to the spectroscopically observed states. Thus, further spectroscopic studies under controlled redox potentials are required for a deeper understanding of the active site interconversions of HoxHY.

Table 3. CO and CN stretching-mode frequencies (in cm^{-1}) of all redox states observed for HoxHY. Numbers in parentheses correspond to the native SH.[23]

Redox state	ν(CO)	ν(CN)	
Ni-Ox	1956	2087	2096
Ni-Ox2	1938	2065	2079
Ni_a-SR	1946 (1946)	n.d. (2080)	n.d. (2090)
Ni_a-SR′	1923 (1922)	2052 (2052)	2069 (2068)
Ni_a-SR2	1956 (1958)	2057 (2068)	2069 (2080)

Conclusions

In the present study we have engineered and characterized the smallest active [NiFe] hydrogenase subcomplex, the heterodimeric hydrogenase moiety, HoxHY, of the bidirectional SH of *R. eutropha*. FTIR spectroscopy reveals a standard set of inorganic ligands for the [NiFe] active site, i.e., one CO and two CN^- ligands coordinated to Fe, as found for the native SH in whole cells.[23] Substoichiometric amounts of FMN in HoxHY were identified by optical spectroscopy, while XAS suggests the presence of a [4Fe4S] cluster. No EPR signature attributable to this cluster was observed under reductive conditions, possibly due to spin coupling with another paramagnetic species. External supply of FMN to HoxHY was found to facilitate reductive reactivation, solution H_2 oxidation activity, and to improve active site stability, suggesting that the cofactor can be reincorporated into the electron pathway of the flavin-deficient enzyme.

The reduced active site states of HoxHY largely resemble those of the native SH in whole cells[23] although the intermediate Ni_a-C state was not detected. FTIR analysis revealed at least two oxidized states in HoxHY, which have not been found in native SH. These differences are likely to be related to the missing FMN and/or the lack of the diaphorase moiety, suggesting a major influence of the electron pathway on the redox behavior of the [NiFe] active site in the SH.

Protein film electrochemistry and solution assays revealed H^+ reduction and H_2 oxidation by HoxHY. The overpotentials relative to $E(2H^+/H_2)$ are minimal and H^+ reduction is less strongly inhibited by H_2 than is observed for the MBH of *R. eutropha* and other O_2-tolerant hydrogenases including the Hyd1 proteins from *E. coli* and *A. aeolicus*.[13–15] The ability of HoxHY to operate close to $E(2H^+/H_2)$ shows that an overpotential is not a requirement for O_2 tolerance. The as-isolated, oxidized enzyme is catalytically inactive and requires reductive activation at potentials close to $E(2H^+/H_2)$. However, no evidence was found for reversible anaerobic oxidative inactivation to yield the Ni_r-B state observed for most other [NiFe] hydrogenases. At high potentials, HoxHY reacts slowly with O_2 to generate an inactive state that can be reactivated within seconds at –384 mV, even in the presence of O_2. Thus, under aerobic conditions in vivo, the low potential imposed by coupling of HoxHY to the NAD^+/NADH pool should be sufficient to preserve H_2 oxidation activity. That is, why – although the SH is sensitive to O_2 at higher potentials – the rapid recovery rate at physiologically relevant lower potentials presumably facilitates O_2-tolerant H_2 oxidation.

Future studies will focus on spectro-electrochemical measurements to elucidate the redox interconversions of HoxHY and assign the active site changes that give rise to distinct inactive states observed in protein film electrochemistry. Site-directed variants of HoxHY will be constructed to investigate the role of residues close to the [4Fe4S] cluster and FMN binding site in order to shed light on the potential role of these cofactors in the function and O_2 tolerance of bidirectional soluble hydrogenases from aerobic H_2-oxidizing bacteria.

Experimental Section

Plasmid Construction and Protein Purification: The overexpression plasmid for purification of the *Strep*-tagged HoxHY module of the *R. eutropha* SH was constructed as follows. We used plasmid pGE617 containing the *hoxFUYWIhypA2B2F2CDEXABCJ* genes under control of the native SH promoter as the basis. An in-frame deletion within the *hoxFU* genes and the introduction of a *Strep*-tagII-encoding sequence to the 5′ end of *hoxY* was established by a previously described genetic replacement strategy[41,42] using plasmids pCH1462 and pCH1440, respectively. Plasmid pCH1462 was constructed by transferring a 2.82 kbp HindIII-BamHI fragment, containing *hoxFU* from pGE15[43] to similarly cut LITMUS 28 (New England Biolabs). In the resulting plasmid, the *hoxFU* in-frame deletion was created by deletion of a 1.5 kbp SalI fragment. Subsequently, a 1.45 kbp XbaI-SalI fragment was inserted into pLO1 yielding pCH1462. For construction of pCH1440, a 1.55 kbp StuI-SacI fragment containing *hoxY* was transferred from pGE15 to SnaBI-SacI-cutted LITMUS 28. For attachment of a *Strep*-tagII to the N-terminus of HoxY, an inverse PCR was applied using the mutagenic primers 5′-GCCCATGGGAGACCCCCCACAAAGACGAGATTGCGTCG-3′ and 5′-GCCCATGGTTTTTCGAACTGCGGGTGGCTCCAAGCCATTTGTCTTCTCCTTCCAGCGCGCG-3′ and the plasmid resulting from the previous step as the template. Finally, a 1.1 kbp StuI-SacI fragment from the resulting amplificate was ligated into equally digested pLO1 yielding pCH1440. Plasmids pCH1462 and pCH1440 were transferred from *E. coli* S17–1 to *R. eutropha* HF210 (pGE617) by conjugation. This allelic exchange procedure yielded strain *R. eutropha* HF788.

R. eutropha HF788 was grown heterotrophically in a mineral salts medium containing a mixture of 0.2% (w/v) fructose and 0.2% (v/v) glycerol (FGN medium)[44] fortified with 1 μM $NiCl_2$ and 1 μM $ZnCl_2$. Large-scale cultivation was performed in 10 L fermenters (Braun Biotech), which were harvested at an optical density at 436 nm of 9 to 11. For the in vivo spectroscopic experiments the strain was grown in 4 L modified FGN medium containing 0.05% fructose and 0.4% glycerol in 5 L baffled Erlenmeyer flasks. The cells were prepared for spectroscopy as described in ref.[23] For purification of HoxHY by affinity chromatography, the cells were resuspended in two volumes of 50 mM Tris-HCl, 150 mM KCl, pH 8.0 buffer containing a protease inhibitor cocktail (EDTA-free Protease Inhibitor, Roche). Cells were broken by two passages through a chilled French pressure cell at 6.2 MPa and the resulting suspension was centrifuged at 100,000 *g* for 45 min. The supernatant (soluble extract) was applied to a 2 mL *Strep*-Tactin Superflow column (IBA), washed with 6 mL of resuspension buffer and eluted with the same buffer containing 5 mM desthiobiotin. Protein fractions containing HoxHY were pooled and concentrated in an Amicon Diaflo cell (YM 30 membrane; Amicon, Witten, Germany).

Biochemistry: The molecular weight of the HoxHY module was determined by size-exclusion chromatography on a Sephadex G-200 column.[45] Hydrogen production was quantified at 30 °C using a modified Clark electrode and reduced MV as the electron donor.[46] The assay chamber was filled with 1.3 mL of N_2-saturated Tris-HCl buffer (50 mM pH 8.0) containing 7.7 mM dithionite and 5 mM MV. For hydrogen oxidation activity, the reduction of MV (5 mM) in 2 mL of H_2-saturated Tris-HCl buffer (50 mM, pH 8.0) was monitored at 30 °C and 605 nm (the molar extinction coefficient of MV is 1.3×10^4 M^{-1} cm^{-1} [47]). Experiments to assess the O_2 tolerance of HoxHY were not possible due to the reoxidation of reduced MV by O_2 in solution assays. To monitor the H_2 oxidation activity a cuvette was filled with H_2-saturated Tris-HCl buffer (50 mM, pH 8.0) containing 5 mM MV and sealed with a rubber stopper. For reductive activation of HoxHY, a 15 μL droplet containing 120 pmol purified protein and 90 nmol dithionite (DT) with (400 pmol) or without FMN was pipetted onto the inner wall of the cuvette. After 30 s the droplet was mixed with the assay buffer, and the H_2-dependent MV reduction was measured spectrophotometrically. For experiments without pre-incubation, 120 pmol HoxHY were directly added to 2 mL of H_2-saturated Tris-HCl buffer (50 mM, pH 8.0) containing 5 mM MV and 45 μM DT. Protein concentrations were determined according to the Bradford method.[48] UV/Vis spectra were recorded with a Varian Cary 300 at 16 °C. SDS-PAGE was performed according to Laemmli et al.[49] For immunological detection of SH-related proteins, the following antisera were applied in the indicated dilutions: anti-HoxH antiserum (1:833), anti-HoxY antiserum (1:1666). Flavin mononucleotide concentrations were analyzed fluorometrically using the method of Schneider et al.[18] modified for a 96-well plate reader (Spectramax M4 spectrofluorometer). Serial dilutions of FMN (73–79% fluorometric grade; Sigma) were used as standard; after previous normalization with a pure FMN sample (approximately 95% by HPLC; Sigma). Quantification of the metal content in protein samples was carried out with a TXRF spectrometer (PicoFox from Bruker).[50] Protein samples (8 μL) were mixed with 8 μL of a 10 mg/L gallium standard (Sigma), 5 μL aliquots were deposited on quarz sample holders which were dried for 20 min at 50 °C and X-ray fluorescence counts were collected for 20 min. Metal concentrations in the protein samples were determined relative to the Ga standard by the build-in routines of the spectrometer.

Electrochemistry: Electrochemical experiments were carried out in a N_2-filled anaerobic glove box (Mbraun < 1 ppm O_2) in a glass electrochemical cell, water-jacketed for temperature control by a water circulator (Grant), and sealed with an o-ring onto an electrode rotator (EG&G model 636). The cell was equipped with gas inlet and outlet fittings to allow exchange of gases in the headspace, and a septum for injection of solutions. Gas-saturated solutions were prepared by bubbling gas into buffer, stored in a thermostatted vial, via needles passing through the septum cap. Accurate gas mixtures were prepared using a manifold of mass flow controllers (Brooks SLA series controlled by Digibox Lite). The counter electrode was a platinum wire, and a Ag/AgCl (3 M NaCl) electrode was employed as the reference. Potentials were converted to volts vs. the standard hydrogen electrode (SHE) using the conversion E(SHE) = E(Ag/AgCl 3 M NaCl) + 0.201 V at 30 °C or + 0.216 V at 10 °C. The electrochemical cell was washed with aqua regia between sets of experiments and then rinsed thoroughly with water. A PGE rotating disk electrode (RDE) with a surface area of 0.03 cm^2 constructed in-house was used as the working electrode. Potentials were controlled using an Autolab128N potentiostat (EcoChemie, Netherlands). Samples of as-isolated HoxHY were stored on ice outside the glove box under aerobic conditions to maintain the as-isolated state. Aliquots of protein (0.7 μL) were taken into the glove box under a N_2 purge immediately prior to formation of a film on

the electrode. To form a protein film, the PGE working electrode was first freshly polished with a slurry of α-alumina (1 μm, Buehler), then rinsed and sonicated for 5 s before application of 0.6 μL of protein which was allowed to adsorb over 1 min. Experiments were carried out in potassium phosphate buffer (50 mM, pH 6.0. 7.0 or 8.0), prepared using MilliQ water (resistivity 18 MΩcm). The volume of electrolyte in the cell was typically 4 mL and the solution was pre-equilibrated with H_2 before insertion of an electrode modified with a film of HoxHY. The electrode was then rotated for a short period before starting an experiment to ensure that the solution was in equilibrium with a known level of H_2. Capacitive current makes a significant contribution to the overall current for low-activity HoxHY films, and cannot easily be removed by subtraction since capacitance differs from one electrode preparation to another and in particular may be significantly different for unmodified and enzyme-modified electrodes. A film of "dead" HoxHY for approximation of the capacitive contribution to current in potential step experiments was prepared by subjecting the film to oxidative damage at 0.5 V.

EPR: EPR measurement were performed as described elsewhere.[23]

FTIR*:* FTIR spectra with a resolution of 2 cm^{-1} were recorded at 10 °C with a Bruker Tensor 27 and IFS28 spectrometer, using a gastight IR cell with CaF_2 windows (ca. 7 μL sample; path length = 50 μm). Incubation of HoxHY with 2–5 mM FMN (10 min) was performed at room temperature in a nitrogen-filled anaerobic glove box. Reduced HoxHY was prepared at room temperature by 30 min incubation with 1 bar H_2 in an anaerobic tent from Coy, filled with forming gas (95–97% N_2, 3–5% H_2). Reductive activation by chemical agents was achieved by incubation with 7.7 mM DT (and 5 mM MV) in a nitrogen filled anaerobic glove box. Absorbance spectra were baseline-corrected using the Bruker OPUS software, version 5.5.

X-ray Absorption Spectroscopy (XAS): XAS measurements were performed at beamline KMC-1 at BESSY (Berlin, Germany). K_α fluorescence-detected XAS spectra at the Fe *K*-edge were collected using a double-crystal (Si111) monochromator on samples held at 20 K in a liquid helium cryostat (Oxford) and employing an energy-resolving 13-element Ge detector (Canberra). XAS spectra were averaged (6–10 scans) after energy calibration of each scan using the first inflection point at 7112 eV in the absorption spectrum of an iron foil as an energy standard. Normalization of spectra and extraction of EXAFS oscillations was performed as described previously.[32] The energy scale of EXAFS spectra was converted to a wavevector (k) scale using an E_0 value of 7112 eV. Unfiltered k^3-weighted spectra were used for least-squares curve-fitting and FT calculation with the in-house program SimX[32] based on phase-functions calculated by FEFF8.4[51] and an amplitude reduction factor (S_0^2) of 0.9.

Supporting Information (see footnote on the first page of this article): Included are the sequence alignment of the HoxY subunit from the *R. eutropha* SH with related hydrogenases and complex I, second derivatives of the FTIR absorbance spectra of Figure 8 (A–F), experiments demonstrating the effect of FMN on enzyme stability, and reductive activations with artificial electron donors with and without H_2. Cyclic voltammograms for HoxHY in the presence and absence of additional FMN are also shown.

Acknowledgments

The work of L. L., O. L., Ma. H., and I. Z. was supported by the Deutsche Forschungsgemeinschaft (DFG) through the Cluster of Excellence "UniCat", Berlin. K. A. V., O. L., J. L., and L. L. are grateful to the Royal Society for an International Joint Project Grant. K. A. V. is a Royal Society Research Fellow and an RCUK Academic Fellow. J. L. is supported by a UK–China Excellence Scheme scholarship. Mi. H. is grateful to the DFG for a Heisenberg Fellowship and for funding (grant Ha3265/3-1), and to the technical staff at BESSY for support. We are indebted to Tanja Burgdorf for construction of plasmid pGE617. We thank Bärbel Friedrich and Peter Hildebrandt for helpful discussions and generous support and Miguel Saggu for EPR analysis of HoxHY.

[1] M. Stephenson, L. H. Stickland, *Biochem. J.* **1931**, *25*, 205–214.
[2] P. M. Vignais, B. Billoud, *Chem. Rev.* **2007**, *107*, 4206–4272.
[3] S. T. Stripp, G. Goldet, C. Brandmayr, O. Sanganas, K. A. Vincent, M. Haumann, F. A. Armstrong, T. Happe, *Proc. Natl. Acad. Sci. USA* **2009**, *106*, 17331–17336.
[4] K. A. Vincent, A. Parkin, F. A. Armstrong, *Chem. Rev.* **2007**, *107*, 4366–4413.
[5] S. E. Lamle, S. P. Albracht, F. A. Armstrong, *J. Am. Chem. Soc.* **2004**, *126*, 14899–14909.
[6] H. Ogata, S. Hirota, A. Nakahara, H. Komori, N. Shibata, T. Kato, K. Kano, Y. Higuchi, *Structure* **2005**, *13*, 1635–1642.
[7] A. Volbeda, L. Martin, C. Cavazza, M. Matho, B. W. Faber, W. Roseboom, S. P. J. Albracht, E. Garcin, M. Rousset, J. C. Fontecilla-Camps, *J. Biol. Inorg. Chem.* **2005**, *10*, 239–249.
[8] A. L. De Lacey, V. M. Fernandez, M. Rousset, R. Cammack, *Chem. Rev.* **2007**, *107*, 4304–4330.
[9] M. Brecht, M. van Gastel, T. Buhrke, B. Friedrich, W. Lubitz, *J. Am. Chem. Soc.* **2003**, *125*, 13075–13083.
[10] V. M. Fernandez, E. C. Hatchikian, R. Cammack, *Biochim. Biophys. Acta* **1985**, *832*, 69–79.
[11] W. Lubitz, E. Reijerse, M. van Gastel, *Chem. Rev.* **2007**, *107*, 4331–4365.
[12] K. A. Vincent, J. A. Cracknell, O. Lenz, I. Zebger, B. Friedrich, F. A. Armstrong, *Proc. Natl. Acad. Sci. USA* **2005**, *102*, 16951–16954.
[13] M. J. Lukey, A. Parkin, M. M. Roessler, B. J. Murphy, J. Harmer, T. Palmer, F. Sargent, F. A. Armstrong, *J. Biol. Chem.* **2010**, *285*, 3928–3938.
[14] M. E. Pandelia, V. Fourmond, P. Tron-Infossi, E. Lojou, P. Bertrand, C. Léger, M. T. Giudici-Orticoni, W. Lubitz, *J. Am. Chem. Soc.* **2010**, *132*, 6991–7004.
[15] K. A. Vincent, J. A. Cracknell, J. R. Clark, M. Ludwig, O. Lenz, B. Friedrich, F. A. Armstrong, *Chem. Commun.* **2006**, 5033–5035.
[16] H. Krassen, A. Schwarze, B. Friedrich, K. Ataka, O. Lenz, J. Heberle, *ACS Nano* **2009**, *3*, 4055–4061.
[17] T. Burgdorf, O. Lenz, T. Buhrke, E. van der Linden, A. K. Jones, S. P. Albracht, B. Friedrich, *J. Mol. Microbiol. Biotechnol.* **2005**, *10*, 181–196.
[18] K. Schneider, H. G. Schlegel, *Biochim. Biophys. Acta* **1976**, *452*, 66–80.
[19] T. Burgdorf, E. van der Linden, M. Bernhard, Q. Y. Yin, J. W. Back, A. F. Hartog, A. O. Muijsers, C. G. de Koster, S. P. Albracht, B. Friedrich, *J. Bacteriol.* **2005**, *187*, 3122–3132.
[20] E. van der Linden, T. Burgdorf, A. L. de Lacey, T. Buhrke, M. Scholte, V. M. Fernandez, B. Friedrich, S. P. Albracht, *J. Biol. Inorg. Chem.* **2006**, *11*, 247–260.
[21] E. van der Linden, B. W. Faber, B. Bleijlevens, T. Burgdorf, M. Bernhard, B. Friedrich, S. P. Albracht, *Eur. J. Biochem.* **2004**, *271*, 801–808.
[22] A. Volbeda, M. H. Charon, C. Piras, E. C. Hatchikian, M. Frey, J. C. Fontecilla-Camps, *Nature* **1995**, *373*, 580–587.
[23] M. Horch, L. Lauterbach, M. Saggu, P. Hildebrandt, F. Lendzian, R. Bittl, O. Lenz, I. Zebger, *Angew. Chem. Int. Ed.* **2010**, *49*, 8026–8029.

[24] T. Burgdorf, S. Löscher, P. Liebisch, E. Van der Linden, M. Galander, F. Lendzian, W. Meyer-Klaucke, S. P. J. Albracht, B. Friedrich, H. Dau, M. Haumann, *J. Am. Chem. Soc.* **2005**, *127*, 576–592.
[25] R. P. Happe, W. Roseboom, G. Egert, C. G. Friedrich, C. Massanz, B. Friedrich, S. P. Albracht, *FEBS Lett.* **2000**, *466*, 259–263.
[26] E. Van der Linden, T. Burgdorf, M. Bernhard, B. Bleijlevens, B. Friedrich, S. P. Albracht, *J. Biol. Inorg. Chem.* **2004**, *9*, 616–626.
[27] K. Schneider, R. Cammack, H. G. Schlegel, *Eur. J. Biochem.* **1984**, *142*, 75–84.
[28] K. Schneider, H. G. Schlegel, K. Jochim, *Eur. J. Biochem.* **1984**, *138*, 533–541.
[29] G. Nöll, *J. Photochem. Photobiol. A: Chem.* **2008**, *200*, 34–38.
[30] J. M. Berrisford, L. A. Sazanov, *J. Biol. Chem.* **2009**, *284*, 29773–29783.
[31] D. E. Edmondson, G. Tollin, *Top. Curr. Chem.* **1983**, *108*, 109–138.
[32] H. Dau, P. Liebisch, M. Haumann, *Anal. Bioanal. Chem.* **2003**, *376*, 562–583.
[33] T. Buhrke, S. Löscher, O. Lenz, E. Schlodder, I. Zebger, L. K. Andersen, P. Hildebrandt, W. Meyer-Klaucke, H. Dau, B. Friedrich, M. Haumann, *J. Biol. Chem.* **2005**, *280*, 19488–19495.
[34] S. Stripp, O. Sanganas, T. Happe, M. Haumann, *Biochemistry* **2009**, *48*, 5042–5049.
[35] K. A. Vincent, N. A. Belsey, W. Lubitz, F. A. Armstrong, *J. Am. Chem. Soc.* **2006**, *128*, 7448–7449.
[36] V. Fourmond, P. Infossi, M. T. Giudici-Orticoni, P. Bertrand, C. Léger, *J. Am. Chem. Soc.* **2010**, *132*, 4848–4857.
[37] K. A. Vincent, A. Parkin, O. Lenz, S. P. Albracht, J. C. Fontecilla-Camps, R. Cammack, B. Friedrich, F. A. Armstrong, *J. Am. Chem. Soc.* **2005**, *127*, 18179–18189.
[38] P. P. Liebgott, F. Leroux, B. Burlat, S. Dementin, C. Baffert, T. Lautier, V. Fourmond, P. Ceccaldi, C. Cavazza, I. Meynial-Salles, P. Soucaille, J. C. Fontecilla-Camps, B. Guigliarelli, P. Bertrand, M. Rousset, C. Léger, *Nat. Chem. Biol.* **2010**, *6*, 63–70.
[39] D. Millo, M. E. Pandelia, T. Utesch, N. Wisitruangsakul, M. A. Mroginski, W. Lubitz, P. Hildebrandt, I. Zebger, *J. Phys. Chem. B* **2009**, *113*, 15344–15351.
[40] F. Germer, I. Zebger, M. Saggu, F. Lendzian, R. Schulz, J. Appel, *J. Biol. Chem.* **2009**, *284*, 36462–36472.
[41] G. Eberz, C. Hogrefe, C. Kortluke, A. Kamienski, B. Friedrich, *J. Bacteriol.* **1986**, *168*, 636–641.
[42] O. Lenz, E. Schwartz, J. Dernedde, M. Eitinger, B. Friedrich, *J. Bacteriol.* **1994**, *176*, 4385–4393.
[43] A. Tran-Betcke, U. Warnecke, C. Bocker, C. Zaborosch, B. Friedrich, *J. Bacteriol.* **1990**, *172*, 2920–2929.
[44] E. Schwartz, U. Gerischer, B. Friedrich, *J. Bacteriol.* **1998**, *180*, 3197–3204.
[45] P. Andrews, *Biochem. J.* **1964**, *91*, 222–233.
[46] A. Schwarze, M. J. Kopczak, M. Rögner, O. Lenz, *Appl. Environ. Microbiol.* **2000**, *76*, 2641–2651.
[47] T. Watanabe, K. Honda, *J. Phys. Chem.* **1982**, *86*, 2617–2619.
[48] M. M. Bradford, *Anal. Biochem.* **1976**, *72*, 248–254.
[49] U. K. Laemmli, *Nature* **1970**, *227*, 680–685.
[50] R. Klockenkämper, *Total-reflection X-ray fluorescence analysis*, Wiley, New York, **1997**.
[51] S. I. Zabinsky, J. J. Rehr, A. Ankudinov, R. C. Albers, M. J. Eller, *Phys. Rev. B* **1995**, *52*, 2995–3009.

Received: October 2, 2010
Published Online: ■

